Peroxidase-like molybdenum oxides/nitrogen-doped graphene quantum dot as the smartphone-based immunosensing probe for the ultrasensitive detection of neurofilament light chain in human serum

Siew Suan Ng[a,c], Ian Sandall[c], Hsin-Cheng Chiu[a]* and Ruey-an Doong[b]*

a.   Department of Biomedical Engineering and Environmental Sciences, National Tsing Hua University, 101, Sec. 2, Kuang Fu Road, Hsinchu 300, Taiwan.

b.   Institute of Analytical and Environmental Sciences, National Tsing Hua University, 101, Sec. 2, Kuang Fu Road, Hsinchu 300, Taiwan.

c.   Department of Electrical Engineering and Electronics, University of Liverpool, Liverpool L69 3BX, United Kingdom.

Corresponding author: Ruey-An Doong (radoong@mx.nthu.edu.tw)

Hsin-Cheng Chiu (hscchiu@mx.nthu.edu.tw)

Abstract

Nanozyme possesses multiple advantages including low cost, high stability, easy manufacture, and versatility, which have earned interest in the application of biomedical purposes. Herein, the nitrogen-graphene quantum dot (N-GQDs) decorated mixed molybdenum oxides (MMO, MoO_x, $2 < x < 3$) were hydrothermally fabricated to serve as the peroxidase-like nanozymes for the ultrasensitive detection of neurofilament light chain (NfL). The kinetics parameters of nanozyme including maximum velocity (V_{max}) and Michaelis-Menten half-saturation constant (K_m) were examined and compared with natural horseradish peroxidase (HRP). In addition, the detection principle of MMO/N-GQD-based immunosensor was established. Results show that addition of N-GQDs can trigger the electron flow from N-GQDs to MMO, making the redox center of Mo elements more effective on electron transfer. The MMO/N-GQDs/PPL/anti-NfL immunosensor exhibits excellent analytical performance on NfL detection with both UV-visible spectrophotometer or smartphone-oriented RGB reader. A linear range of 16 to 1000 pg mL^{-1} with a limit of detection of 2.24 pg mL^{-1} and recovery of 83 – 104 % in human serum is achieved. The immunosensor can attain a selectivity coefficient of higher than 0.7 against interferences containing common ions, amino acids, cholesterol, and biomarkers in serum. Results corroborate that the green-synthesized peroxidase-like MMO/N-GQD possesses the advantages of cost-effective and high scalability, which can serve as a potential nanozyme to replace natural enzyme for the ultrasensitive and selective detection of serum NfL with superior recovery in human serum.

2

1. Introduction

The development of civilization as well as the good medical environment has made the human life longer than at any previous time. According to the World Health Organization, it is estimated that 2.1 billion people aged > 60 and 426 million people aged > 80 years old will be achieved by the year 2050 [1]. Aging will then be a significant risk factor for neurodegenerative disorders, and, therefore, the rapid and accurate detection of neurodegenerative diseases plays a pivotal role in addressing the early alarming issue [2]. Currently, the clinical diagnosis of the neurodegenerative disorder is based on the behavioral assessment, bioimaging, or molecular diagnostics. More recently, the search of serum biomarkers, such as neurofilament light chain (NfL), to serve as biomolecules for neurodegenerative disorder diagnostics or prognosis has received much interest [3-6]. However, the sacred amount of NfL has made the detection difficult. Therefore, an ultrasensitive, patient-centered diagnostic tool targeting the serum biomarker is urgently needed.

Nanozyme, which uses nanomaterial as a biomimetic enzyme, has proven as an effective sensing probe with several advantages including low cost, high stability, easy manufacture, and versatility, which have earned interest in the application of biomedical purposes [7, 8]. Nanomaterials can undergo different kinds of reactions, which can be mimicked to enzymes like peroxidase, oxidase, and superoxide dismutase. The peroxidase-like nanozyme can oxidize organics like 3, 3', 5, 5'-tetramethylbenzeme (TMB) in the presence of H_2O_2 in a very short time, enabling speedy screening of targeted biomarkers. Several nanomaterials have been reported as peroxidase-like nanozyme, such as metal oxide [9], noble metal [10, 11], metal composites [12, 13], carbon derivatives [14, 15], and metal-organic-framework [16] for the detection of metal ions [14, 17], organic contaminants or bioactive ingredients [12, 16], and biomolecules [9, 13].

However, the use of peroxidase-based nanozymes for sensing of biomolecules mainly focuses on metabolites, and the application to disease biomarker sensing has still been underestimated.

Graphene quantum dots (GQDs) are carbon derivatives with low-cost, abundant, and highly conductive. The tiny size of GQDs has enhanced the quantum confinement and edge effects, leading to a well-defined spin multiplicity of the electronic states. As a result, GQDs have more splitting in electron-hole gaps, further enabling a speedy electron transfer rate [18, 19]. GQDs are usually oxidatively reactive, which are highly relevant to be peroxidase mimics under ambient conditions as they have oxygen-containing functional groups in attachment to the electrophilic species [20]. However, the quantum size of GQD limits its direct utilization and catalytic efficiency because of the low colloidal stability [21]. Therefore, a solid support is needed to improve the catalytic performance of GQDs.

Several carbon-based nanomaterials such as carbon nanotube, graphene, and porous materials have been employed as the solid support in sensing application because of the high specific surface area and good conductivity. However, one of the main issues of these carbonaceous materials is the limited hydrophilicity, which can greatly affect on the sensitivity of the biomimic sensor. Instead, metal oxides exhibit certain credits such as redox reactivity and high surface area or volume, which can act as the support to enhance the catalytic performance of GQDs [22]. Mixed molybdenum oxides (MMO, MoO_x, $2 < x < 3$) have beneficial properties including good hydrophilicity, high affinity towards oxygen, high electron mobility, low resistivity, high melting point, and high chemical stability [23-25], which has been widely used in the catalysis [26, 27], sensing [28, 29], energy storage applications [30, 31]. However, the decoration of N-doped GQDs onto MMO as the sensing probe of immunosensor for the ultrasensitive detection of degenerative biomarker, NfL, has received less attention.
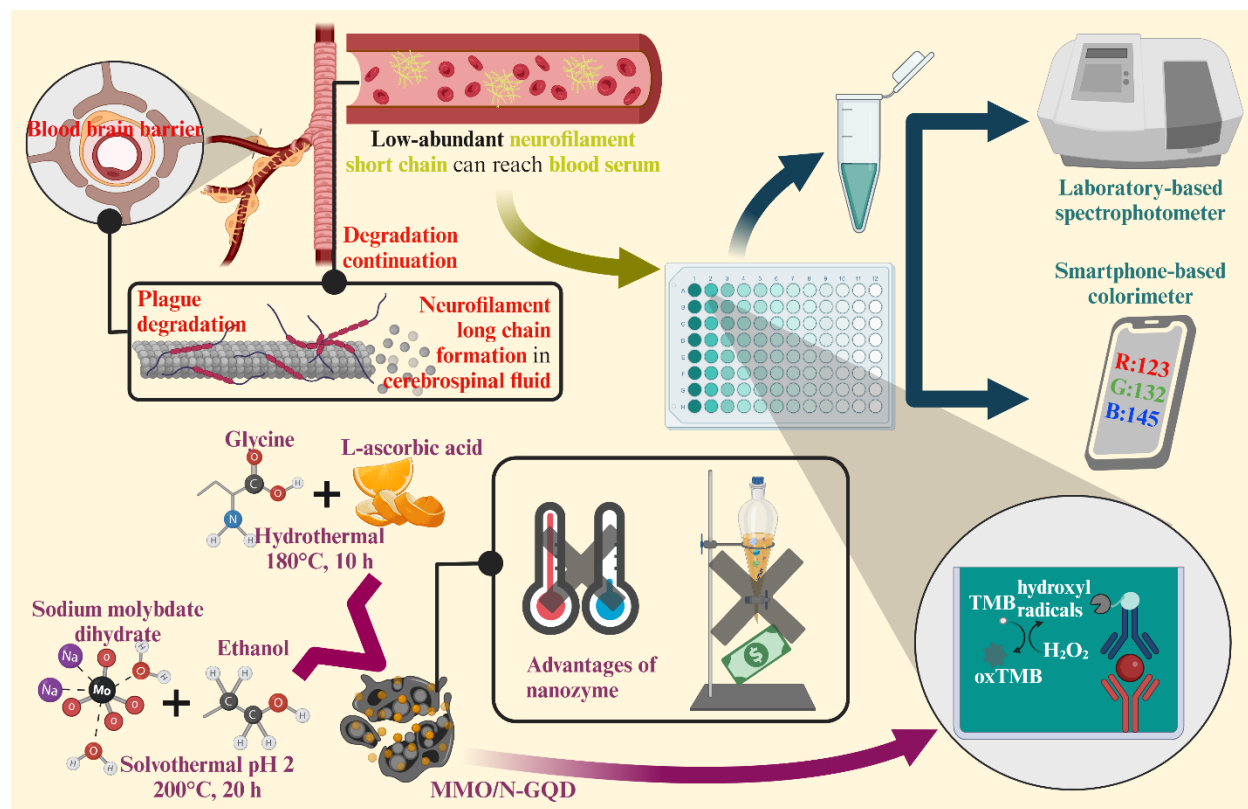
Scheme 1. Schematic diagram of peroxidase-like colorimetric detection of serum NfL.

Herein, the N-GQDs were homogeneously decorated onto the MMO surface to serve as the biomimic sensing probe of immunosensor for the optical detection of NfL in human serum. As illustrated in Scheme 1, the MMO, prepared by the solvothermal method at pH 2, was mixed with glycine and L-ascorbic acid at 180 °C for 10 h to form MMO/N-GQDs nanocomposites. The MMO/N-GQDs were then anchored with anti-NfL to form the immunosensor. The MMO/N-GQDs exhibit the excellent peroxidase activity, and induce the color change in the presence of TMB and H_2O_2. The catalytic activity of MMO/N-GQDs including maximum reaction rate (V_m) and Michaelis-Menten affinity constant (K_m) was determined and compared with natural peroxidase. Moreover, the MMO/N-GQDs/anti-NfL show superior sensitivity and selectivity toward human NfL detection. In addition, the signal caused from the color change was detected

5

using spectrophotometer and smartphone-based RGB reader. The purpose of recording results in gray value is to reserve its applicability as smart diagnostics after incorporating with machine learning in the future. Results show that an ultrasensitive nanozyme-mediated immunosensor for detecting serum NfL has been successfully developed which can open an avenue for optical-based biosensor to detect NfL and other neurodegenerative diseases.

2. Experimental

The detailed experimental section including materials and reagents, preparation of MMO/N-GQDs nanocomposites, catalytic activity of MMO/N-GQDs, setup of the smartphone-based colorimetric sensor, and application for NfL detection in serum can be found in Supplementary Materials. In addition, the detection and selectivity of NfL are described below

2.1. Detection and selectivity of NfL

A 96-well plate was used to detect NfL by natural antibody and as-prepared MMO/N-GQDs/PLL/anti-NfL. A 100 µL of NfL sample was added to each well and incubated at 37 °C. The liquid was decanted, and 50 µL of biotinylated anti-NfL and MMO/N-GQD/PLL/anti-NfL were added to react for the natural peroxidase and nanozyme sets, respectively.

For the natural peroxidase set, the biotinylated anti-NfL was added with 100 µL of HRP conjugate, and incubated for 30 min at room temperature. The resulting plates for natural peroxidase set were decanted and washed with buffer for five times. Then, they were incubated in the 96-well plate for 1 h at room temperature. The liquid was removed and the plate was washed with buffer 3 times. The substrate solution was added to the plate and incubated for 15 min at room temperature, and then the stop solution was added to terminate the reaction.

For MMO/N-GQDs/PPL/anti-NfL detection, 100 µL of 1 mM H_2O_2, 150 µL of 0.1 M acetate buffer at pH 3.5, and 50 µL of 0.01 M TMB were added to the nanozyme set, and then incubated for 2.5 min. The absorbance of resulting solution for both the natural enzyme and nanozyme set at 650 nm was determined and recorded.

## 3. Results and discussion

3.1. Characterization of MMO/N-GQDs

The XRD patterns of molybdenum oxide shows a binary mixture oxide of MoO_2 and MoO_3. As illustrated in Fig. S1, the (011), (100), (111), (114), (017) and (217) planes of MoO_3, which correspond to 2θ of 23.3°, 23.6°, 33.4°, 41.4°, 49.9°, and 72.2°, respectively, are found in the synthesized MMO. Besides, peaks at 2θ of 26.2°, 37.5°, 38.9°, 53.9°, 61.3°, 65.0°, and 77.9° are resulting from the crystal planes of (011), (101), (111), (022), (031), (211) and (132) planes of MoO_2, respectively. The crystalline properties of MMO/N-GQDs are further characterized by using XRD and Raman spectroscopy. The amorphous peak of N-GQD at 20° – 25° 2θ is not observed due to the higher signal of well-crystalline MMO (Fig. S2). However, the Raman spectrum of N-GQD signal shows the D-band and G-band of graphene derivatives at 1358 and 1596 cm^{-1} (Fig. 1a), indicating that the N-GQDs has been successfully decorated onto the MMO.

The FTIR spectra were recorded to confirm the functional groups on the nanocomposite. As observed in Fig. 1b, the FTIR spectrum can be divided into four regions: A, B, C, and D. For region A, the peak of N-HR$_2$ group in the range of 2700 – 3000 cm^{-1} becomes visible after decorating MMO with N-GQDs. Moreover, the stretching of the R-NH$_2$ group in the range of 1600 – 1800 cm^{-1} (region B) becomes visible after addition of N-GQDs onto metal oxide. In contrast, the Mo-OH group in region C becomes less visible in the presence of N-GQDs, which can conclude that

the adsorbed water has been reduced as the composite is occupied with N-GQDs. Lastly, peaks of the O-Mo-O, Mo-O, and Mo=O bonds in the range of 650–1000 cm^{-1} appear in the composite (region D). The chemical composition of MMO/N-GQDs was further identified by XPS analysis. As depicted in Fig. 1c, the XPS of MMO shows O 1s (532 eV), Mo 3s (509 eV), Mo 3p (395–412 eV), and Mo 3d (228–233 eV). A trace amount of C 1s (284 eV) is mainly attributed to the air contaminant during preparation. The appearance of In 3d peak is mainly attributed to the role as standard to obtain a more accurate chemical shift due to the catalytic activity. The pure N-GQDs show peaks at 532, 400, and 284 eV, which are the characteristic peaks of N-GQDs. The decoration of N-GQDs onto MMO exhibits all the peaks of N-GQDs and MMO, elaborating the successful fabrication of MMO/N-GQDs nanocomposites.

To further understand the chemical species of elements in MMO, N-GQD, and MMO/N-GQDs, the XPS peaks of carbon (C), nitrogen (N), molybdenum (Mo) and oxygen (O) were deconvoluted. It can be seen that the four peaks including C=C, C-C, C-N/C-O, and C=O are clearly observed in the deconvoluted C 1s peaks of N-GQDs and MMO/N-GQDs (Fig. S3a). The O 1s peaks of all the materials contain C=O and C-O-C peaks (Fig. S3b), indicating the hydrophilic properties of N-GQDs and MMO/N-GQDs [32]. The deconvoluted Mo spectra show Mo (IV) and Mo (VI) peaks (Fig. S3c), which in good agreement with the HRTEM result. Moreover, graphitic-N, pyridinic-N and pyrrolic-N appear in the N-GQDs and MMO/N-GQDs (Fig. S3d), corroborating the successful doping of N atoms into GQDs. It is interesting that the pyridinic-N peak shifts to the high binding energy after the decoration of N-GQDs onto MMO, clearly indicating that the MMO receives electrons from N-GQDs, and leads to the increase in the charge density of MMO. The reduced states of M-O bonds may create more reactive sites for MMO/N-GQDs nanocomposites to enhance biosensing sensitivity.
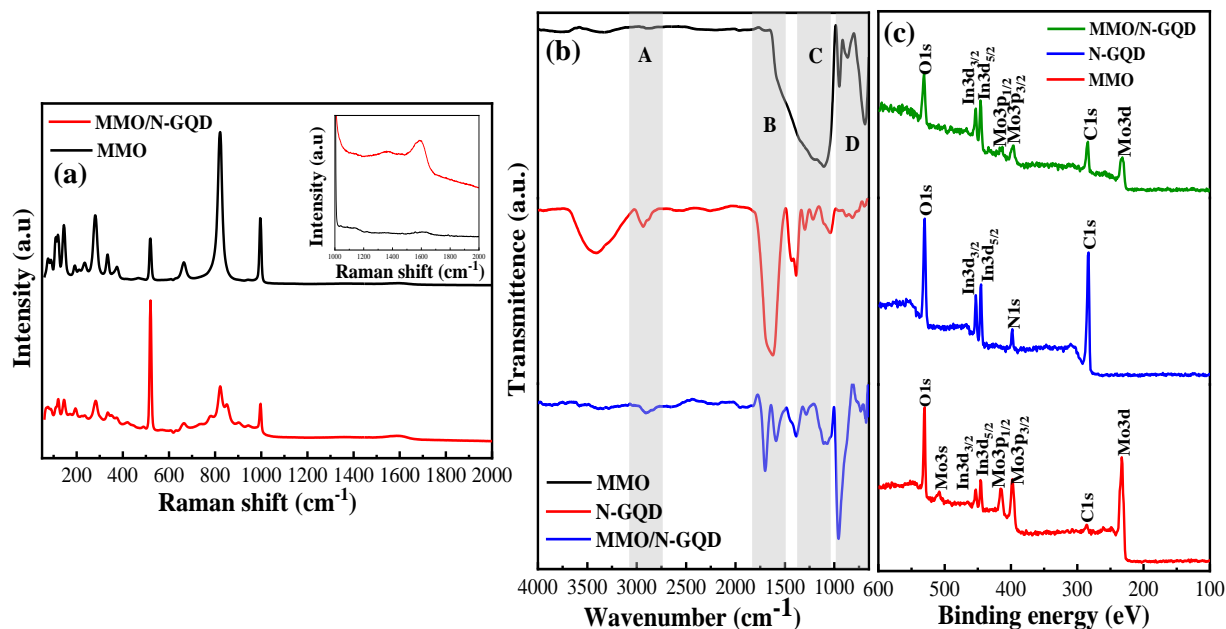
Fig. 1. (a) The Raman spectra of pure MMO and MMO/N-GQDs, (b) the ATR-FTIR spectra and (c) the XPS spectra of MMO, N-GQDs, and MMO/N-GQDs.

The morphology of the MMO/N-GQDs was examined by the HRTEM image. Generally, the as-synthesized MMO/N-GQD is sheet-like with d-spacing of 0.24 nm, which can be referred as the (111) crystal lattice of MoO_2 (Fig. S4) [33]. In addition, a d-spacing of 0.36 nm, which represents the (001) crystal plane of MoO_3 is also observed [34, 35]. The induced EDS mapping shown in Fig. S5 also indicates the presence of Mo, O, C and N elements with nitrogen content of 2.4 at% in the nanocomposite.

3.2. Feasibility of MMO/N-GQD as peroxidase and its mechanisms

The biomimicking behavior of MMO/N-GQD was first examined with TMB and H_2O_2 as the substrates. As shown in Fig. S6, no peak is observed in the absence of MMO/N-GQDs nanozymes (control). As the peroxidase-like MMO/N-GQD can react with H_2O_2, the resulting radicals will

further oxidize TMB, giving rise to the formation of oxidized TMB to produce a blue complex at absorption wavelength of 650 nm.

The catalytic activity as well as catalytic parameter of MMO/N-GQD was determined via Michaelis-Menten kinetics study. Fig. 2 shows the the Michaelis-Menten curves as a function of TMB and H_2O_2 concentrations, and the catalytic activity of MMO/N-GQDs increases rapidly upon the increase in substrate concentrations (Figs 2a and 2b). In addition, the Lineweaver–Burk relationship was plotted to determine the V_{max} and K_m. A good linear relationship between $1/V$ and $1/[S]$ is obtained (inset of Figs. 2a and 2b). Therefore, the V_{max} and K_m can be deduced as 3.99×10^{-8} M s^{-1} and 0.089 mM for TMB, and 6.1×10^{-8} M s^{-1} and 0.020 mM, respectively, for H_2O_2. The lower K_m value towards H_2O_2 in comparison with TMB indicates that the MMO/N-GQD nanozyme has a better affinity towards H_2O_2.

The peroxidase activity of MMO/N-GQDs in the presence of TMB and H_2O_2 is summarised in Fig. 2c. The acid buffer provides the H_2O_2 an ideal supporting factor for the formation of hydroxide ions, while also enabling the nanozyme to turn into π-cation radicals. The unstable π-cation radicals react with the hydroxide ions readily, forming the oxidized nanozyme and radicals. Next, the oxidized nanozyme returns to its reduced form by further reacting with the H_2O_2, giving out more radicals. These radicals would then react with TMB to yield a blue oxidized complex, which can produce strong absorption intensity at 650 nm.

Table S2 compares the Michaelis-Menten constants of MMO/N-GQDs with the other previously reported nanozymes. Several nanomaterials including iron oxide, Co_3O_4, Co_3S_4, MoS_2, mesoporous carbon, and MOF have been used as nanozymes to trigger the oxidation of TMB in the presence of H_2O_2. It is clear that the obtained K_m values (0.02 – 0.089 mM) are lower than most of the other studies, and the V_{max} values [$(3.99 – 6.1) \times 10^{-8}$ M s^{-1}] is higher those reported

results shown in Table S2 [36-41]. It is noticeable that the V_{max} of MMO/N-GQDs is lower than that of HPR. However, both the K_m values of TMB and H_2O_2 for MMO/N-GQDs are lower than that of HRP, signifying the high affinity of MMO/N-GQDs toward TMB and H_2O_2. These results clearly indicate that the as-prepared MMO/N-GQDs can be used as a potential alternative for natural HRP to trigger the oxidation of TMB, which can serve an excellent sensing probe of the immunosensor for the detection of NfL in human serum.
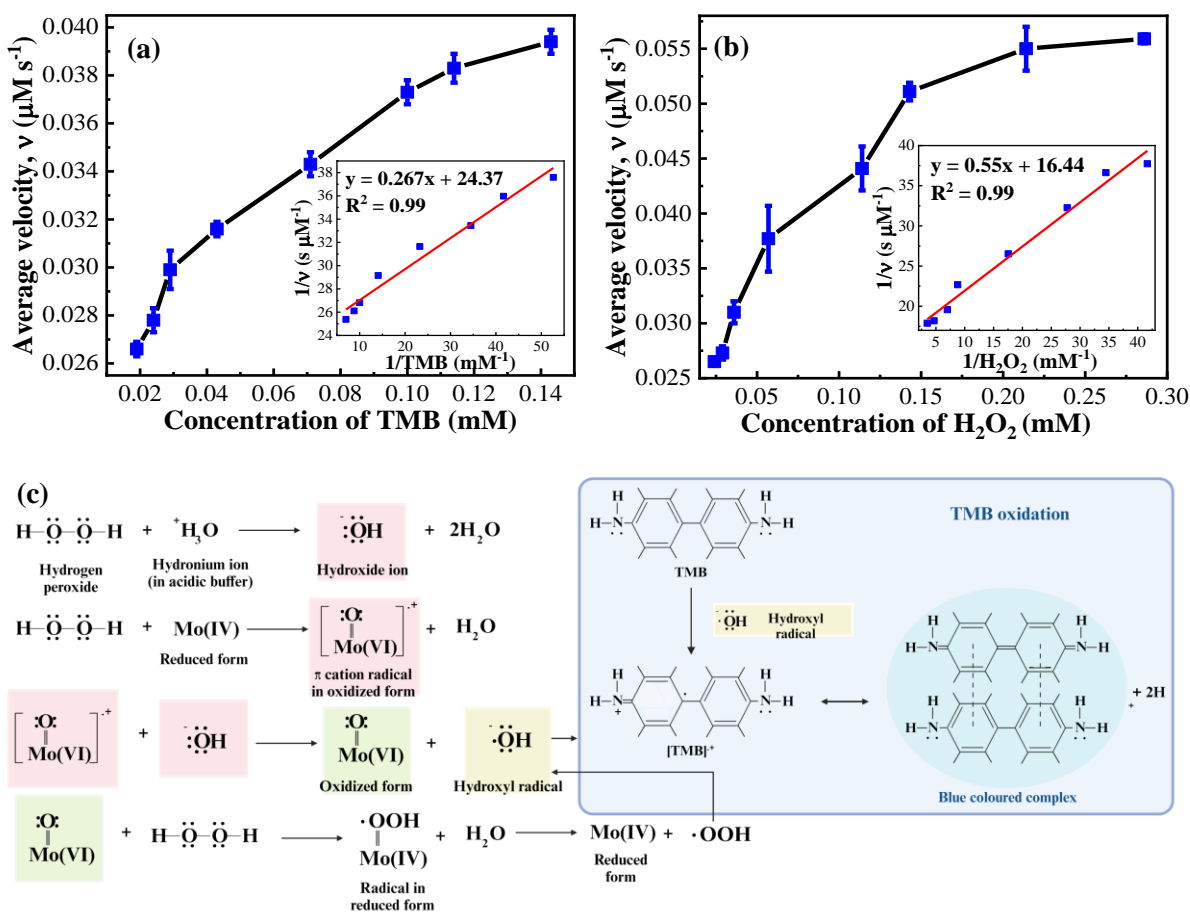
Fig. 2. The Michaelis-Menten plots of reaction between MMO/N-GQD and (a) TMB and (b) H_2O_2, and (c) the proposed mechanism for the biomimicking MMO/N-GQDs reaction in the presence of H_2O_2 and TMB. Inset is the Lineweaver–Burk plot between MMO/N-GQDs and TMB or H_2O_2.

3.3. Advantages of MMO/N-GQD over natural enzymes

Natural enzymes like hydrogen peroxidase (HRP) are used in biotechnological processes and wastewater treatment, but their catalytic performance is limited at ambient conditions. Nanozymes like MMO/N-GQDs can serve as a better alternative due to their higher tolerance to temperature and pH. The wastewater or environmental conditions are commonly existed under the harsh conditions (i.e. hotter weather at 50 °C while colder weather at 10 °C; the domestic wastewater is usually acidic while the industrial wastewater can be alkali). The study evaluated the catalytic activity of MMO/N-GQDs nanozyme under different conditions such as TMB and H_2O_2 concentrations, the added amount of nanozyme, buffer pH, and temperature (Table S1), comparing it with natural peroxidase. The nanozyme shows similar behavior to natural peroxidase, but with high catalytic activity at 50 °C and pH 4. The nanozyme is considered as a better substitute for natural enzyme HRP due to its easier scalability, cheaper cost, and more environmentally friendly synthetic process. Organic solvents used in natural enzymes are toxic and costly.

3.4. Optimization of parameters for NfL detection

After the surface characterization and the demonstration of the validity of MMO/N-GQDs as the suitable sensing probe, the MMO/N-GQDs was further undergone surface modification with PPL, and then anchored with anti-NfL to form the immunosensor. Fig. S7a shows the change in the surface zeta potential of the sensing probe during the surface modification and biofunctionalization. Initially, the surface charge of the MMO/N-GQD is negative (-38 mV). Then, the surface negativity reduces to -5 mV after the modification with PLL. The SEM image (Fig. S7b) clearly shows the big lumps under the same magnification after the modification with PLL in comparison with MMO/N-GQDs nanocomposites. This phenomenon indicates that the

MMO/N-GQD is composed of a polycationic polymer. Furthermore, the electrostatic interaction between nanozyme with anti-NfL enhances during the biofunctionalization, resulting in the change in zeta potential of MMO/N-GQDs/PPL/anti-NfL to the positive charges of 5 mV.
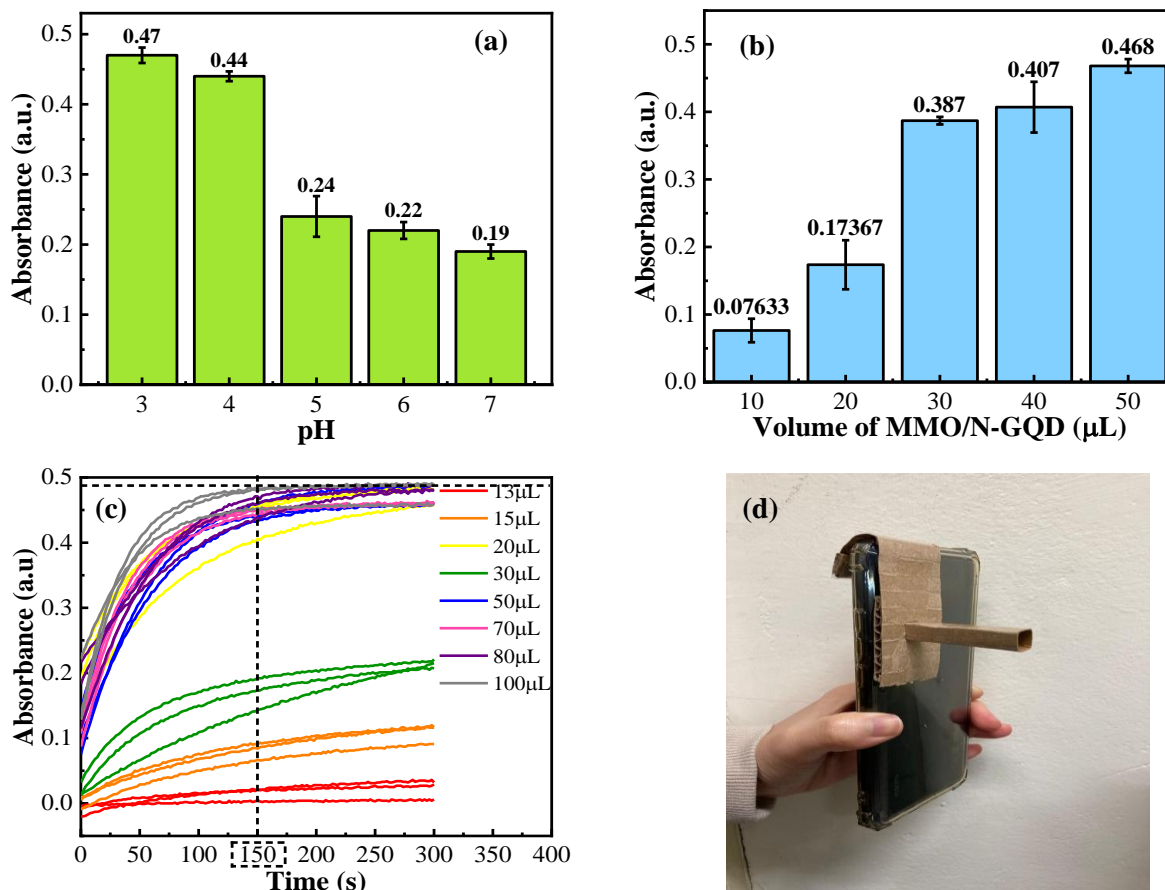
Fig. 3. (a) The UV-Vis spectra that are resulted from buffer with different pH, (b) The UV-Vis spectra that are resulted from the different volume of nanozyme, (c) The UV-Vis spectra of various concentrations for 300 s, and (d) The prototype and interface of the smartphone-based colorimeter.

The sensing parameters including buffer pH, added volume of nanozyme, and the incubation period for the chromogenic development were studied. Generally, the setting that gives the maximum absorbance at 650 nm was determined as the optimized parameter. Firstly, the pH of

buffer is optimized by varying the solution pH from 3 to 7. Then, the optimized pH is justified to be 4 as it gives the highest precision and relatively high absorbance (Fig. 3a). Although pH 3 shows the highest absorbance, the low pH could reduce the colloidal stability of antibody as the active site of antigen or antibody may be deaminated [42, 43]. Next, the optimized nanozyme volume has determined to be 50 µL with the highest absorbance and favorable precision (Fig. 3b). Moreover, the incubation time for the chromogenic development is optimized as 2.5 min as the absorbance reaches its saturation state (Fig. 3c). After the optimization, these optimized parameters are applied to detect NfL in serum using both a spectrophotometer and a smartphone-based colorimeter (Fig. 3d).

3.5 Detection of NfL in PBS buffer

Fig. 4a display the detection of NfL using MMO/N-GQDs/PPL/anti-NfL immunosensor at 650 nm. The wavelength intensity of 650 nm decreases as the NfL concentration increases, clearly signifying the successful detection of NfL using nanozyme-based immunosensors. Moreover, the detection of NfL using immunosensor with HRP as the sensing probe was also examined. As shown in Fig. 4b, the maximum absorbance wavelength of 442 nm decreases upon the increase in NfL concentration (Fig. 4b), validating the feasibility of using MMO/N-GQDs/PPL/anti-NfL immunosensor for NfL detection. Both the absorbance at the maximum wavelength of 650 nm for nanozyme and 442 nm for HRP can be translated into the linear plot as a function of NfL concentration. As displayed in Fig. 4c, two linear relationship between absorbance and $\log(C_{NfL})$ with a correlation coefficient of > 0.99 are clearly observed. The linear relationship of $ABS = 0.35 \log(C_{NfL}) - 0.38$ for HRP and $ABS = 0.31 \log(C_{NfL}) - 0.37$ for MMO/N-GQDs nanozyme is obtained. The similar linear relationship between HRP and nanozyme clearly indicates that the as-

prepared MMO/N-GQD is an excellent sensing probe which can potentially replace the natural HRP to effectively detect NfL in human serum.
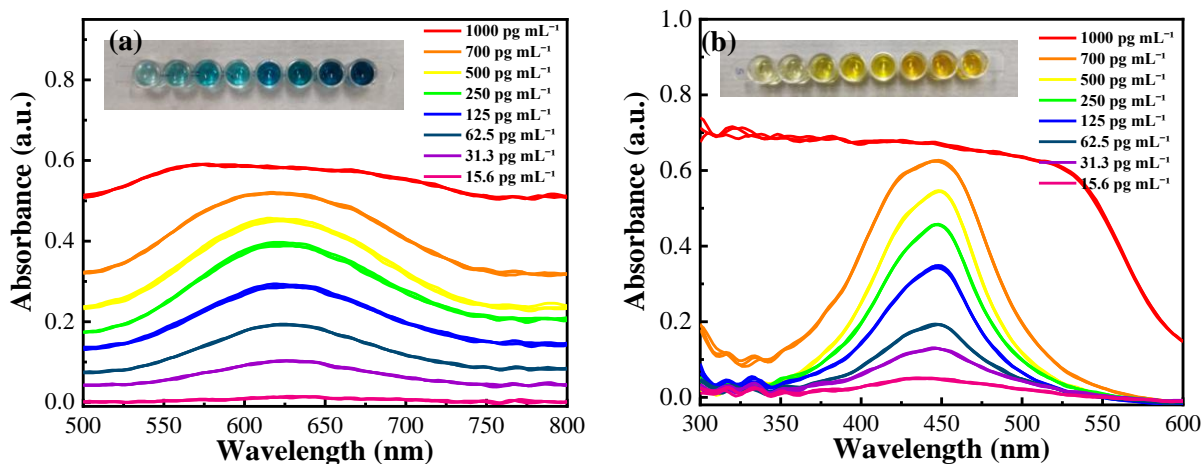
Fig. 4. The UV-Vis spectra of (a) MMO/N-GQDs nanozyme and (b) HRP.

The detection of NfL by using a smartphone-based colorimeter was also validated, indicating the potential for remote sensor applications. The color change is recorded as grey values, with intensity varying with intensity. The darker the intensity of the color, the lower grey value is obtained. Green color is chosen due to human eye photoreceptor sensitivity, resulting in maximum color intensity.

Fig. 5a shows the linear relationship between the grey value and NfL concentration detected with a smartphone-based colorimeter. An inversely proportional relationship of $ABS = -0.183 \log(C_{NfL}) + 237.9$ ($R^2 = 0.99$) is established. Therefore, it is noticeable that the slope of the linear relationship using laboratory-orientated spectrophotometer is higher than that of the smartphone-based colorimeter, depicting that the UV-visible spectrophotometer is still more sensitive than the proposed colorimeter. However, the good linear relationship with excellent correlation coefficient validates the feasibility of using smartphone-oriented device to rapid and accurate detection of NfL and other neurodegenerative biomarker in human serum.

The limit of detection (LOD), determined from the 3× relative standard deviation after 7 replicates of lowest NfL concentration applied, is calculated as 2.24 pg mL^{-1} with a relative standard deviation as low as 4.5% for the laboratory-orientated spectrophotometer set using nanozyme, whereas 4.22 pg mL^{-1} with a relative standard deviation as low as 4.5% for the smartphone-based colorimeter set using nanozyme. It indicates that the developed immunosensor is sensitive enough to detect a significant minimum NfL amount in human serum. The usual range of serum NfL concentration of an adult below 50 years old is approximately 20 pg mL^{-1}. The elevation of serum NfL concentration with the course of aging can be as high as 50 pg mL^{-1} [44]. Thus, it is clearly that the LOD for this immunosensor is 10 times lower than the normal amount of serum NfL, which is suitable to serve as a screening tool for the diagnostic or prognosis of NfL and neurodegenerative disorders in human serum.

In order to justify the selectivity of immunosensors toward NfL detection, 10 different interferants were added in the presence and absence of the analyte of interest (NfL). The interferants include common ions, amino acids, lipids, proteins, and biomarkers in human serum. The selectivity obtained from a UV-visible spectrophotometer is shown in Fig. 5b. The selectivity coefficient has been calculated by taking the blank human serum and the control without interferant as the references. Thus, it is deducible that the designated immunosensor is highly selective towards NfL with a selectivity coefficient higher than 0.7. Moreover, all the selectivity coefficients of the system in the absence of analyte but only the interferant including blank human serum are lower than 0.3. The selectivity study has been also determined by the smartphone-based colorimeter (Fig. 5c). The window for RGB signal is only fall within the small range of 1 – 255. It is getting saturated at a high intensity with less fluctuation in the RGB scale obtained. Thus, the error bars may be too minor to be observed. This simple design is due to the limitation of RGB

system, as the signal window is limited from 1 – 255, which is unlike the UV-visible spectrophotometer intensity system that has unlimited y-axis signal window. The result indicates that the selectivity coefficient of system with a mixture of interferant and analyte is higher than 0.8. In contrast, the selectivity of the system without analyte and the blank human serum is higher than 2. This is because the gray value intensity is inversely proportional to the absorbance value. Thus, the overall result corroborates that the innovated immunosensor is highly selective towards the analyte of interest, NfL with significantly low interferences from other biomolecules.

The color change during NfL detection is primarily due to redox reactions between the nanozyme and substrates. Thus, the chemical shift of the elements in the peroxidase-like MMO/N-GQDs nanozyme before and after the reaction was examined via XPS analysis. The peroxidase-like colorimetric reaction involves two steps: hydroxyl radical production as H_2O_2 is reduced into H_2O and O_2, and oxidization of TMB. As can be seen in Fig. S8a, the Mo 3d species such as (VI), (IV) and (0) in the nanozyme shifts back to the low binding energy in the system containing TMB. The binding energy of $Mo3d_{3/2}$ shifts from 234.5 to 235.6 eV without TMB, indicating the occurrence of oxidation reaction. In contrast, the $Mo 3d_{3/2}$ shifts from 235.8 to 235.2 eV again after the addition of TMB, which indicates that the reduction happens. Therefore, the phenomenon further justifies the role of MMO/N-GQD nanozyme acts as a catalyst in the peroxidase-like reaction, as its oxidation state is conserved after a chemical reaction. The hydroxyl radicals are much more reduced in the system with TMB in comparison to that without TMB in the EPR analysis (Fig. S8b), further indicates hydroxyl radicals are used in TMB oxidation. The increase in analyte attached has also elevated the intensity of radicals as there is more nanozyme accompanied along with the capture antibody (Fig. S8c). Therefore, it is deducible that the

MMO/N-GQD nanozyme can act as a catalyst for the radical production out of H_2O_2 followed by the oxidation of TMB.
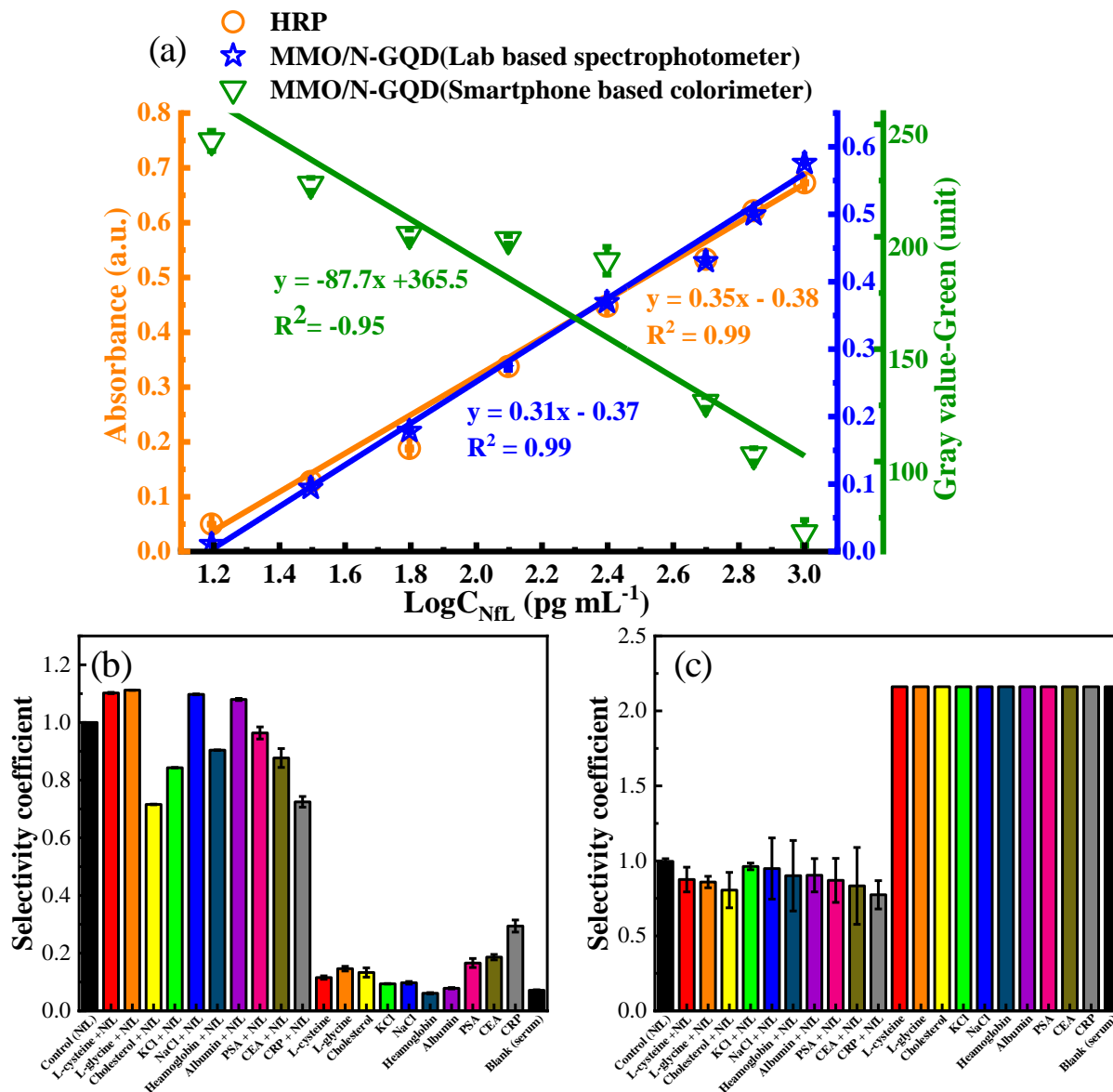
Fig. 5. (a) The linear plot of the HRP, MMO/N-GQDs using a spectrophotometer and, the MMO/N-GQDs nanozyme using smartphone-based colorimeter. The selectivity of MMO/N-GQD immunosensor using (b) spectrophotometer and (c) smartphone-based colorimeter.

3.6 Application for NfL detection in serum and recovery

Table S3 shows the recovery of the colorimetric immunosensor for NfL detection in human serum. The recoveries of 83 – 104% with a significantly low relative standard deviation of 0.8 – 4.7 % can be achieved. Therefore, this colorimetric immunosensor is feasible in real cases. The innovated immunosensor has potential be applied in real human sample with the significant high recovery and low standard deviation.

4. Conclusions

In this study, a peroxidase-like MMO/N-GQDs nanozyme has been successfully fabricated with the hydrothermal method at 180 °C for 10 h, and then serve as the optical sensing probe of immunosensor for the ultrasensitive and selective detection of NfL in human serum. Through the Michaelis-Menten kinetic study, the MMO/N-GQD exhibits low K_m and the high V_{max}, and the catalytic activity of MMO/N-GQD is similar to the HRP. Moreover, the nanozyme shows excellent catalytic activity under extreme conditions at low pH of 4 and high temperature of 50 °C. Moreover, the MMO/N-GQDs/PPL/anti-NfL immunosensors can effectively detect NfL with UV-visible spectrophotometer or smartphone-oriented colorimeter. Under the optimized condition, the MMO/N-GQD based immunosensor exhibit excellent analytical performance toward NfL detection in human serum with a dynamic range of 3 orders of magnitude. Furthermore, the developed immunosensor achieves relatively low LOD of 2.24 pg mL^{-1} and high recovery of 83 – 104% in real serum samples within a short duration. Moreover, the possible detection mechanism for NfL detection has been developed and proven. Results of this study signify the successful preparation of MMO/N-GQDs nanozyme as the optical sensing probe of immunosensor for effective detection of NfL, which can pave a path to develop the metal oxide-based nanozyme with

high sensitivity and selectivity for the effective detection and diagnosis of NfL and other neurodegenerative disorders.

Acknowledgements

Appendix A. Supplementary data

Supplementary data to this article can be found online at:

References

[1] WHO. "Ageing and health." WHO. https://www.who.int/news-room/fact-sheets/detail /ageing-and-health (accessed June 25, 2022).

[2] M. N. S. Karaboğa, M. K. Sezgintürk, Biosensor approaches on the diagnosis of neurodegenerative diseases: Sensing the past to the future, J. Pharm. Biomed. Anal. 209 (2022) 114479. https://doi.org/10.1016/j.jpba.2021.114479.

[3] L. Gaetani, K. Blennow, P. Calabresi, M. Di Filippo, L. Parnetti, H. Zetterberg, Neurofilament light chain as a biomarker in neurological disorders, J. Neurol. Neurosurg. Psychiatry 90(8) (2019) 870-881. https://doi.org/10.1136/jnnp-2018-320106.

[4] M. A. Jacob, N. Peters, M. Cai, M. Duering, S. T. Engelter, J. Kuhle, F. E. de Leeuw, A. M. Tuladhar, Increased neurofilament light chain is associated with increased risk of long-lerm mortality in cerebral small vessel disease, J. Stroke 24(2) (2022) 296-299. https://doi.org/10.5853/jos.2021.04385.

[5] M. Pekny, U. Wilhelmsson, A. Stokowska, T. Tatlisumak, K. Jood, M. Pekna, Neurofilament light chain (NfL) in blood-A biomarker predicting unfavourable outcome in the acute phase and improvement in the late phase after stroke, Cells 10(6) (2021) 1537. https://doi.org/10.3390/cells10061537.

[6] T. Uphaus, S. Bittner, S. Gröschel, F. Steffen, M. Muthuraman, K. Wasser, M. Weber-Krüger, F. Zipp, R. Wachter, K. Gröschel, NfL (Neurofilament Light Chain) levels as a predictive marker for long-term outcome after ischemic stroke, Stroke 50(11) (2019) 3077-3084. https://doi.org/10.1161/strokeaha.119.026410.

[7] C. Hong, X. Meng, J. He, K. Fan, X. Yan, Nanozyme: A promising tool from clinical diagnosis and environmental monitoring to wastewater treatment, Particuology 71 (2022) 90-107. https://doi.org/10.1016/j.partic.2022.02.001.

[8] D. Jiang, D. Ni, Z. T. Rosenkrans, P. Huang, X. Yan, W. Cai, Nanozyme: new horizons for responsive biomedical applications, Chem. Soc. Rev. 48(14) (2019) 3683-3704. https://doi.org/10.1039/C8CS00718G.

[9] S. Ali, S. Sikdar, S. Basak, D. Das, D. Roy, M. S. Haydar, V. K. Dakua, P. Adhikary, P. Mandal, M. N. Roy, Synthesis of β-cyclodextrin grafted rhombohedral-CuO antioxidant nanozyme for detection of dopamine and hexavalent chromium through off–on strategy of peroxidase mimicking activity, Microchem. J. 179 (2022) 107514. https://doi.org/10.1016/j.microc.2022.107514.

[10] X. Liao, X. Zhao, Z. Tan, C. Wang, W. Liu, Au nanoparticles in 2D bimetallic metal–organic frameworks with enhanced plasmonic nanozyme activity for antibacterial therapy, ACS Appl. Nano Mater. 5(11) (2022) 16145–16153. https://doi.org/10.1021/acsanm.2c03049.

[11] Y. Li, L. Wang, Z. Cui, S. Liu, S. Wang, J. Ren, Y. Tian, R. Shu, X. Luo, Y. Liao, J. Wang, White peroxidase-mimicking nanozyme-nanocarrier of enzyme labeled antibody to enhance catalytic performance and relieve color interference of immunoassay, Sens. Actuators B Chem. 364 (2022) 131909. doi: https://doi.org/10.1016/j.snb.2022.131909.

[12] C. B. Ma, Y. Xu, L. Wu, Q. Wang, J. J. Zheng, G. Ren, X. Wang, X. Gao, M. Zhou, M. Wang, H. Wei, Guided synthesis of a Mo/Zn dual single-atom nanozyme with synergistic effect and peroxidase-like activity, Angew. Chem. Int. Ed. 61(25) (2022) e202116170 https://doi.org/10.1002/anie.202116170.

[13] S. Naveen Prasad, S. R. Anderson, M. V. Joglekar, A. A. Hardikar, V. Bansal, R. Ramanathan, Bimetallic nanozyme mediated urine glucose monitoring through discriminant analysis of colorimetric signal, Biosens. Bioelectron. 212 (2022) 114386. https://doi.org/10.1016/j.bios.2022.114386.

[14] J. Goswami, L. Saikia, P. Hazarika, Carbon dots-decorated g-C_3N_4 as peroxidase nanozyme for colorimetric detection of Cr(VI) in aqueous medium, ChemistrySelect 7(31) (2022) e202201963 https://doi.org/10.1002/slct.202201963.

[15] Q. Li, H. Li, K. Li, Y. Gu, Y. Wang, D. Yang, Y. Yang, L. Gao, Specific colorimetric detection of methylmercury based on peroxidase-like activity regulation of carbon dots/Au NPs nanozyme, J. Hazard. Mater. 441 (2023) 129919. https://doi.org/10.1016/j.jhazmat.2022.129919.

[16] K. Zhang, L. Lu, Z. Liu, X. Cao, L. Lv, J. Xia, Z. Wang, Metal-organic frameworks-derived bimetallic oxide composite nanozyme fiber membrane and the application to colorimetric detection of phenol, Colloids Surf. A Physicochem. Eng. Asp. 650 (2022) 129662. https://doi.org/10.1016/j.colsurfa.2022.129662.

[17] G. Zhang, K. Yu, B. Zhou, J. Wang, C. Zheng, L. Qu, H. Chai, X. Zhang, Magnetic zirconium-based Prussian blue analog nanozyme: enhanced peroxidase-mimicking activity and colorimetric sensing of phosphate ion, Microchim. Acta 189(6) (2022) 220. https://doi.org/10.1007/s00604-022-05311-8.

[18] S. Zhu, Y. Song, J. Wang, H. Wan, Y. Zhang, Y. Ning, B. Yang, Photoluminescence mechanism in graphene quantum dots: Quantum confinement effect and surface/edge state, Nano Today 13 (2017) 10-14. https://doi.org/10.1016/j.nantod.2016.12.006.

[19] A. Sheely, B. Gifford, S. Tretiak, A. Bishop, Tunable optical features of graphene quantum dots from edge functionalization, J. Phys. Chem. C 125(17) (2021) 9244-9252. https://doi.org/10.1021/acs.jpcc.1c00537.

[20] H. Sun, Y. Zhou, J. Ren, X. Qu, Carbon nanozymes: Enzymatic properties, catalytic mechanism, and applications, Angew. Chem., Int. Ed. 57(30) (2018) 9224-9237. https://doi.org/10.1002/anie.201712469.

[21] Q. Li, B. Chen, B. Xing, Aggregation kinetics and self-assembly mechanisms of graphene quantum dots in aqueous solutions: Cooperative effects of pH and electrolytes, Environ. Sci. Technol. 51(3) (2017) 1364-1376. https://doi.org/10.1021/acs.est.6b04178.

[22] Paras, K. Yadav, P. Kumar, D. R. Teja, S. Chakraborty, M. Chakraborty, S. S. Mohapatra, A. Sahoo, M. M. Chou, C. T. Liang, D. R. Hang, A review on low-dimensional nanomaterials: nanofabrication, characterization and applications, Nanomaterials 13(1) (2022) 160. https://doi.org/10.3390/nano13010160.

[23] Y. Shi, B. Guo, S. A. Corr, Q. Shi, Y. S. Hu, K. R. Heier, L. Chen, R. Seshadri, G. D. Stucky, Ordered mesoporous metallic MoO_2 materials with highly reversible lithium storage capacity, Nano Lett. 9(12) (2009) 4215-4220. https://doi.org/10.1021/nl902423a.

[24] O. Concepción and O. de Melo, The versatile family of molybdenum oxides: synthesis, properties, and recent applications, J. Phys. Condens. Matter 35(14) (2023) 143002. https://doi.org/10.1088/1361-648X/acb24a.

[25] I. A. de Castro, R. S. Datta, J. Z. Ou, A. Castellanos-Gomez, S. Sriram, T. Daeneke, K. Kalantar-zadeh, Molybdenum oxides – from fundamentals to functionality, Adv. Mater. 29(40) (2017) 1701619. https://doi.org/10.1002/adma.201701619.

[26] Y. Liu, J. Li, A. Das, H. Kim, L. O. Jones, Q. Ma, M. J. Bedzyk, G. C. Schatz, Y. Kratish, T. J. Marks, Synthesis and structure–activity characterization of a single-site MoO_2 catalytic center anchored on reduced graphene oxide, J. Am. Chem. Soc. 143(51) (2021) 21532-21540. https://doi.org/10.1021/jacs.1c07236.

[27] F. Gaspar, C. D. Nunes, Selective catalytic oxidation of benzyl alcohol by MoO_2 nanoparticles, Catalysts 10(2) (2020) 265. https://doi.org/10.3390/catal10020265.

[28] F. An, S. Mu, S. Zhang, W. Xu, N. Li, H. Wang, S. Wang, C. Zhao, J. Feng, L. Wang, B. Sun, MoO_2 Nanospheres synthesized by microwave-assisted solvothermal method for the detection of H_2S in wide concentration range at low temperature, Front. Mater. 8 (2021) 670044. https://www.frontiersin.org/articles/10.3389/fmats.2021.670044.

[29] X. Song, M. Yin, J. Li, Y. Li, H. Yang, Q. Kong, H. Bai, G. Xi, L. Mao, Moving MoO_2/C nanospheres with the functions of enrichment and sensing for online-high-throughput SERS detection, Anal. Chem. 94(19) (2022) 7029-7034. https://doi.org/10.1021/acs.analchem.2c00043.

[30] H. Wang, X. Jiang, Y. Wang, X. Yang, Y. Chai, Z. Yu, M. Xu, R. Yuan, Constructing 3D MoO_2/N-doped carbon composites with amorphous nanowires and crystalline nanoparticles for high Li storage capacity, Powder Technol. 377 (2021) 281-288. https://doi.org/10.1016/j.powtec.2020.09.001.

[31] J. Li, J. Wang, F. Jiao, Y. Lin, Y. Gong, Heterostructured CoP/MoO_2 as high efficient electrocatalysts for hydrogen evolution reaction over all pH values, Int. J. Hydrog. Energy 46(35) (2021) 18353-18363. https://doi.org/10.1016/j.ijhydene.2021.03.011.

[32] H. L. Tran, V. D. Dang, N. K. Dega, S.-M. Lu, Y.-F. Huang, R.A. Doong, Ultrasensitive detection of breast cancer cells with a lectin-based electrochemical sensor using N-doped graphene quantum dots as the sensing probe, Sens. Actuators B: Chem. 368 (2022) 132233. https://doi.org/10.1016/j.snb.2022.132233.

[33] Q. Bkour, C. M. Cuba-Torres, O. G. Marin-Flores, S. Tripathi, N. Ravishankar, M. G. Norton, S. Ha, Mechanistic study of the reduction of MoO_2 to Mo_2C under methane pulse conditions, J. Mater. Sci. 53(18) (2018) 12816-12827. https://doi.org/10.1007/s10853-018-2549-0.

[34] D. Xiang, C. Han, J. Zhang, W. Chen, Gap states assisted MoO_3 nanobelt photodetector with wide spectrum response, Sci. Rep. 4(1) (2015) 4891 https://doi.org/10.1038/srep04891.

[35] L. Guo, L. Cao, J. He, J. Huang, Y. Wang, J. Li, K. Kajiyoshi, S. Chen, Inducing [100]-orientated plate-like α-MoO_3 to achieve regularly exfoliated layer structure enhancing Li storage performance, J. Mater. 32(3) (2021) 3006-3018. https://doi.org/10.1007/s10854-020-05052-5.

[36] M. Amirzehni, H. Eskandari, B. Vahid, J. Hassanzadeh. An efficient chemiluminescence system based on mimic $CuMOF/Co_3O_4$ nanoparticles composite for the measurement of glucose and cholesterol, Sens. Actuators B: Chem. 348 (2021) 130690.

[37] P. Borthakur, P. K. Boruah, P. Das, M. R. Das. 2021. CuS nanoparticles decorated MoS2 sheets as an efficient nanozyme for selective detection and photocatalytic degradation of hydroquinone in water, New J. Chem.45 (2021) 8714-27.

[38] S. Hashmi, M. Singh, P. Weerathunge, E. L. H. Mayes, P. D. Mariathomas, S. N. Prasad, R. Ramanathan, V. Bansal, Cobalt sulfide nanosheets as peroxidase mimics for colorimetric detection of l-cysteine, ACS Appl. Nano Mater. 4 (2021) 13352-62.

[39] Y. Q. Liu, J. Q. Li, A. Das, H. Kim, L. O. Jones, Q. Ma, M. J. Bedzyk, G. C. Schatz, Y. Kratish, T. J. Marks, Synthesis and structure–activity characterization of a single-site MoO_2 catalytic center anchored on reduced graphene oxide, J. Am. Chem. Soc. 143 (2021) 21532-40.

[40] X. Zhang, Z. Zhang, Y. Cao, W. Tang, Z. Li, Co–Mn mixed metal oxide nanorods for on-site colorimetric detection of SO_3^{2-} in food samples. ACS Appl. Nano Mater. 5 (2022) 6810-19.

[41] M. A. Wahab, S. M. A. Hossain, M. K. Masud, H. Park, A. Ashok, M. Mustapić, M. Kim, D. Patel, M. Shahbazi, M. S. A. Hossain, Y. Yamauchi, Y. V. Kaneti, Nanoarchitectured superparamagnetic iron oxide-doped mesoporous carbon nanozymes for glucose sensing, Sens. Actuators B: Chem. 366 (2022) 131980.

[42] D. Ejima, K. Tsumoto, H. Fukada, R. Yumioka, K. Nagase, T. Arakawa, J. S. Philo, Effects of acid exposure on the conformation, stability, and aggregation of monoclonal antibodies, Proteins 66(4) (2007) 954-962. https://doi.org/10.1002/prot.21243.

[43] M. E. Alam, G. V. Barnett, T. R. Slaney, C. G. Starr, T. K. Das, P. M. Tessier, Deamidation can compromise antibody colloidal stability and enhance aggregation in a pH-dependent manner, Mol. Pharm. 16(5) (2019) 1939-1949. https://doi.org/10.1021/acs.molpharmaceut.8b01311.

[44] M. Khalil, L. Pirpamer, E. Hofer, M. M. Voortman, C. Barro, D. Leppert, P. Benkert, S. Ropele, C. Enzinger, F. Fazekas, R. Schmidt, Serum neurofilament light levels in normal aging and their association with morphologic brain changes, Nat. Commun. 11(1) (2020) 812. https://doi.org/10.1038/s41467-020-14612-6.